European Journal of Pharmacology xxx (xxxx) 175349

Contents lists available at ScienceDirect

European Journal of Pharmacology

journal homepage: www.elsevier.com/locate/ejphar

Efficacy of selective histone deacetylase 6 inhibition in mouse models of *Pseudomonas aeruginosa* infection: A new glimpse for reducing inflammation and infection in cystic fibrosis

Margherita Brindisi [a, 1, *], Simona Barone [a], Alice Rossi [b], Emilia Cassese [a], Nunzio Del Gaudio [c], Álvaro Javier Feliz Morel [d], Gessica Filocamo [d], Alessia Alberico [a], Ida De Fino [b], Davide Gugliandolo [b], Mehrad Babaei [c], Guglielmo Bove [c], Martina Croce [e], Camilla Montesano [e], Lucia Altucci [c], Alessandra Bragonzi [b], Vincenzo Summa [a, 1, **]

[a] *Department of Pharmacy, Department of Excellence 2018-2022, School of Medicine and Surgery, University of Naples "Federico II", Via D. Montesano 49, I-80131, Naples, Italy*

[b] *Infections and Cystic Fibrosis Unit, Division of Immunology, Transplantation and Infectious Diseases, IRCCS San Raffaele Scientific Institute, Via Olgettina 60, 20132, Milano, Italy*

[c] *Department of Precision Medicine, University of Campania Luigi Vanvitelli, Vico L. de Crecchio 7, 80138, Naples, Italy*

[d] *Exiris s.r.l., Via di Castel Romano, 100, 00128, Rome, Italy*

[e] *Department of Chemistry, Sapienza University of Rome, Piazzale Aldo Moro 5, 00185, Rome, Italy*

ARTICLE INFO

Keywords:
Histone deacetylase 6
Cystic fibrosis
Epigenetics
Lung
Inflammation
Infection
Mouse model

ABSTRACT

The latest studies identified the histone deacetylase (HDAC) class of enzymes as strategic components of the complex molecular machinery underlying inflammation in cystic fibrosis (CF). Compelling new support has been provided for HDAC6 isoform as a key player in the generation of the dysregulated proinflammatory phenotype in CF, as well as in the immune response to the persistent bacterial infection accompanying CF patients. We herein provide *in vivo* proof-of-concept (PoC) of the efficacy of selective HDAC6 inhibition in contrasting the pro-inflammatory phenotype in a mouse model of chronic *P. aeruginosa* respiratory infection. Upon careful selection and in-house re-profiling (*in vitro* and cell-based assessment of acetylated tubulin level through Western blot analysis) of three potent and selective HDAC6 inhibitors as putative candidates for the PoC, we engaged the best performing compound **2** for pre-clinical studies. Compound **2** demonstrated no toxicity and robust anti-inflammatory profile in a mouse model of chronic *P. aeruginosa* respiratory infection upon repeated aerosol administration. A significant reduction of leukocyte recruitment in the airways, in particular neutrophils, was observed in compound **2**-treated mice in comparison with the vehicle; moreover, quantitative immunoassays confirmed a significant reduction of chemokines and cytokines in lung homogenate. This effect was also associated with a modest reduced bacterial load after compound **2**-treatment in mice compared to the vehicle. Our study is of particular significance since it demonstrates for the first time the utility of selective drug-like HDAC6 inhibitors in a relevant *in vivo* model of chronic *P. aeruginosa* infection, thus supporting their potential application for reverting CF phenotype.

1. Introduction

Cystic fibrosis (CF) patients harbor mutations of the cystic fibrosis transmembrane conductance regulator (CFTR) gene coding for a cyclic AMP-regulated chloride ion channel accounting for the faulty transport of the chloride ion across the surface of epithelial cells (Bye et al., 1994). This, in turn causes, defective defence mechanisms against microorganisms, prompting severe airway infections in CF patients (Boucher, 2004). CF-associated infection of the respiratory tract fea-

* Corresponding author.
** Corresponding author.
E-mail addresses: margherita.brindisi@unina.it (M. Brindisi), vincenzo.summa@unina.it (V. Summa).
[1] Co-senior authors

https://doi.org/10.1016/j.ejphar.2022.175349
Received 6 August 2022; Received in revised form 17 October 2022; Accepted 20 October 2022
0014-2999/

tures the coexistence of multiple bacterial species, thus further complicating the selection of an effective antibiotic treatment.

Members of the multidrug-resistant "ESKAPE" pathogens group such as *Pseudomonas aeruginosa* and *Staphylococcus aureus* (including methicillin resistant *S. aureus* [MRSA]), are most frequently isolated from the sputum of patients with CF. A plethora of virulence factors produced by *P. aeruginosa* can play a pivotal role in the establishment of chronic infections and inflammation in CF patients (Zobell et al., 2012). Therefore, molecules able to restore an efficient immune response are of great interest in the treatment of polymicrobial infections in CF.

The initial stage of CF-related lung disease is mainly characterized by prolonged airway inflammation, mucus hypersecretion and oxidative stress (Bodas et al., 2018; Vij et al., 2009; Wagner et al., 2016). Evolution to chronic disease stage entails recurrent infection with *P. aeruginosa* and permanent pulmonary impairment, thus triggering the collapse of respiratory function (Castellani and Assael, 2017). Chronic inflammation in CF is mainly associated with NFκB mediated proinflammatory signaling and neutrophil chemotaxis (Bodas et al., 2018; Wagner et al., 2016). Beyond neutrophils, other innate and adaptive immune cells are associated with increased levels of pro-inflammatory cytokines and chemokines, thus promoting CF-lung disease (Nichols and Chmiel, 2015). Since CFTR-targeted therapies showed swinging efficacy in reducing inflammation in CF airways, a complementary safe and effective anti-inflammatory treatment to be administered in conjunction with CFTR correctors and potentiators would represent an unvaluable benefit for CF patients. Additionally, CF patients featuring CFTR mutations not responsive to available modulators, would at least benefit from innovative therapeutic options re-establishing inflammatory regulation.

The latest studies identified the histone deacetylase (HDAC) class of enzymes as strategic components of the complex molecular machinery underlying inflammation in CF. In particular, compelling new support has been provided for HDAC6 isoform as a key player in the generation of the dysregulated proinflammatory and fibrotic phenotype in CF (Brindisi et al., 2020; Rymut et al., 2013, 2017; Bodas et al., 2018; Rosenjack et al., 2019; Shan et al., 2008). HDAC6 has also been shown to play a pivotal role in bacterial clearance or killing, directly ascribable to its ability in modulating CF immune responses (Rosenjack et al., 2019). Inhibiting HDAC6 functions may represent a novel and effective strategy for tackling multiple aspects of CF-associated lung disease. Selective HDAC6 inhibition should also avoid the common toxicities related to the currently available unselective HDAC inhibitors (Lee et al., 2015; Brindisi et al., 2018; Zhang et al., 2021).

In this study, we have set up an appropriate screening funnel of selective HDAC6 inhibitors and provided the first *in vivo* proof-of-concept (PoC) of the efficacy of selective HDAC6 inhibition in contrasting the pro-inflammatory phenotype in a mouse model *P. aeruginosa* respiratory infection. First, we embarked a careful compound selection by performing a thorough analysis of scientific literature and relevant patents in the field to match the product profile. Three short-listed candidates displaying high HDAC6 inhibitory potency and relevant selectivity profile over other HDAC isoforms were selected as the reference compounds to be putative candidates for the PoC study, taking into account also the physicochemical properties, available information on DMPK profile and synthetic feasibility. The compounds were synthesized first in small scale to assess in-house their potency and selectivity in the enzymatic assays and in the cell-based assays (A549 and HeLa cells) to assess the ability to selectively increase acetyl-tubulin levels compared to acetyl-histone levels as markers of selectivity for the cytoplasmic form of HDAC6 and nuclear isoforms, and also the cytotoxicity. The delivery method was chosen to be aerosol to maximize the exposure in the lung and hopefully reduce systemic circulation and potentially the toxicity, this method resembles the human administration for the CF patients, for this reason, the compound solubility in the vehicle was one of the selection criteria. Based on the comparison of the compounds overall profile, compound **2** was selected as the best candidate to be further advanced in the *in vivo* assessment on acute and chronic mouse models of *P. aeruginosa* infection. Indeed, compound **2** demonstrated no toxicity and robust anti-inflammatory profile in a mouse model of *P. aeruginosa* infection upon aerosol administration. In conclusion, compound **2** proved to be the first agent safe and efficacious in an *in vivo* efficacy PoC study for the selective HDAC6 inhibitor in the mouse model *P. aeruginosa* respiratory infection that recapitulates the bacterial infection in CF.

2. Materials and methods

2.1. Toxicity and efficacy of compound **2** in mouse model of P. aeruginosa acute and chronic lung infection

Toxicity evaluation of different doses of compound **2** was tested in C57BL/6NCrl male mice (Charles River), 8–10 weeks old. Mice were maintained under specific pathogen-free conditions in sterile cages in a ventilated isolator. Compound **2** (5, 10 and 20 mg/kg) or vehicle (PBS + DMSO 4%) were administered aerosol by Penn Century 18h before and 5 min after PBS inoculation. Before each treatment and, 6 h and 24 h post PBS inoculation, mice were weighted and their body temperature measured, in order to evaluate general health status. Mice were sacrificed 24 h after second treatment.

To evaluate the efficacy of compound **2,** C57BL6/NCrl male mice (8–10 weeks old) (Charles River) were anesthetized by an intraperitoneal (i.p.) injection of 2.5% Avertin (2,2,2-tribromoethanol, 0.015 ml/g body weight) and infected by intratracheal (i.t.) injection of planktonic 1×10^6 *P. aeruginosa* PAO1 reference strain for acute infection or 4–5x10^5 *P. aeruginosa* MDR-RP73 clinical strain embedded in agar beads for chronic infection. In acute infection, mice were treated with compound **2** 18 h before infection and 5 min after the infection, by aerosol administration using Penn Century MicroSprayer® Aerosoliser device with different doses (5, 10 and 20 mg/kg or PBS + 4% DMSO as vehicle). In the chronic infection model, the treatment started 5 min after the infection with repeated daily doses for 3 or 7 days. Health status and change in body weight were monitored daily. After 6 h from acute infection or 3 and 7 days from the chronic infection, mice were monitored for lung colony-forming units (CFUs) and cell counts in the bronchoalveolar lavage fluid (BALF) as described previously (Facchini et al., 2014; Kukavica-Ibrulj et al., 2014).

Blood was collected from the retro-orbital sinus by penetrating sterile hematocrit capillary tube into EDTA-treated tubes. Cells were removed from plasma by centrifugation 10000 rpm 5 min at room temperature. Plasma was stored at −80 °C. Cytokine/chemokine levels were measured in the supernatant of lung homogenates by Bioplex Assay (Bio-Rad Laboratories, Segrate, Italy).

2.2. Histone deacetylase 6 (HDAC6) inhibitors

2.2.1. Chemical synthesis

For the synthesis of novel HDAC6 inhibitors, starting materials were purchased from commercial suppliers and used without further purification. TLC analysis was conducted using aluminum foil supported thin-layer silica gel chromatography plates (F254 indicator). Column chromatography was performed using 230–400 mesh, 60 Å pore diameter silica gel. For ^{1}H NMR and ^{13}C NMR measurements an accurately weighed amount of analyte (about 5.0–10.0 mg) was dissolved in 600 μL of deuterated chloroform ($CDCl_3$) or dimethyl sulfoxide (DMSO-d_6). The mixture was transferred into a 5 mm NMR tube and the spectra were acquired on a Bruker Advance 400 MHz or 700 MHz spectrometers by using the residual signal of the deuterated solvent as internal standard. Splitting patterns are described as singlet (s), doublet (d), triplet (t), quartet (q) and broad (br); the values of chemical shifts (δ) are given in ppm and coupling constants (*J*) in Hertz (Hz). NMR data

were processed with MestreNova (Version 8.1.1, Mestrelab Research). ESI-MS spectra analysis was carried out on a mass spectrometer LTQ-XL. HPLC was performed with a Waters Model 510 pump equipped with Waters Rheodyne injector and a differential refractometer, model 401. Luna 5 μm PFP (2) 100A HPLC Column 250 × 10 mm was employed. The purity of compounds was estimated to be greater than 95% by HPLC analysis. Optical rotation values were measured at room temperature operating at λ = 589 nm, corresponding to the sodium D line, and were determined in a Jasco P-200 (Jasco Europe s.r.l., Cremella, Italy) polarimeter using a microcell (1 mg sensitivity) containing the compound dissolved in 1 mL of chloroform.

The chemical synthesis and characterization of compounds **1–3** is described in the Supplementary Information.

2.2.2. Solubility determination

Each compound was dissolved in dimethyl sulfoxide (DMSO) at a concentration of 10 mM. Then, 10 μL of the obtained solution was diluted either in 490 μL of PBS pH 7.4 or MeOH and maintained under agitation at 250 rpm for 24 h at room temperature. Tubes were subsequently centrifuged for 5 min at 4000 rpm and 10 μL of each sample were further diluted in 490 μL of MeOH and analyzed by LC–MS/MS. The ratio of mass signal area obtained in PBS and in organic solvent was then calculated and used to determine the solubility of each compound.

2.2.3. Enzymatic assays

Protocol 1: Synthesized HDAC6 selective inhibitors were characterized through Fluorogenic HDAC6 Assay Kit. The kit was purchased from BPS Bioscience (San Diego, CA). The assays were carried out in black NUNC 96-well plates according to the supplier's instructions. Briefly: candidate HDCA6 inhibitors were dissolved at various concentrations (0.005, 0.01, 0.05, 0.1, 0.5, 1, 2.5, and 5 μM) in HDAC assay buffer (BPS Bioscience, Catalog #: 50031), containing HDAC 1 or 6 enzymes (HDAC-1: 0.033 mg/ml, BPS Bioscience, Catalog #: 50051 and HDAC-6 0.025 mg/mL, BPS Bioscience, Catalog #: 50006), BSA (1 mg/mL, Sigma-Aldrich), and HDAC substrate 3 (200 μM, BPS Bioscience, Catalog #: 50037). SAHA (0.5 μM, Merck) was used as inhibitor control. The enzymatic reaction was then incubated at 37 °C for 30 min. Subsequently, HDAC assay developer (50 μL, BPS Bioscience, Catalog #: 50030) was added to the reaction and incubated at room temperature for 15 min. The fluorescence was recorded at excitation and emission wavelengths of 360 and 460 nm, respectively. The positive controls (Fp) and enzyme-free controls (Fb) were defined as 100% and 0% of HDAC activity, respectively. The percent activity of each compound was calculated as (F - Fb)/(Fp - Fb), where F is the value of fluorescence intensity at the indicated concentration of the compound. Prism (GraphPad Software, La Jolla, CA) software was used to calculate IC_{50}.

Protocol 2: The enzyme, either HDAC1 (His-FLAG-tagged # 50051, BPS Biosciences, San Diego, CA, USA) or HDAC6 (GST-tagged, #50006, BPS Biosciences, San Diego, CA, USA) was incubated for 30 or 60 min, respectively, at 30 °C in assay buffer (25 mM TrisCl pH 8.0, 130 mM NaCl, 0,05% Tween20, 10% Glycerol, 1 mg/mL of BSA and 2.7 mM KCl in the case of HDAC6) in the presence of different concentrations of HDAC inhibitors. Then FLUOR DE LYS®-Green substrate (BML-KI572-0050, Enzo Biochem, New York, NY, USA) was added to a final concentration of 150 or 15 μM respectively and incubated for 30 or 60 min respectively at 30 °C. The reaction was stopped using the developer solution (2X), containing 2 μM of TSA, a dilution 1:200 of FLUOR DE LYS® developer I concentrate (BML-KI105-0300, Enzo Biochem, New York, NY, USA) diluted in development buffer (50 mM TrisCl pH 8.0, 137 mM NaCl, 2,7 mM KCl and 1 mM MgCl2). Fluorescence was measured using VICTOR Nivo Multimode Microplate Reader, using excitation filter 480/30 nm and emission filter 530/30 nm. After subtraction of background fluorescence (enzyme-free samples), the percentage of activity of each concentration point was calculated vs positive controls (inhibitor-free samples). Cell viability was analyzed with GraphPad software applying a curve fitting nonlinear regression model.

2.3. Cell treatments

For the viability assay, HeLa cells were seeded into 96-well plate at 2000 cells/well in triplicate. The day after compounds were added to the wells in complete culture medium in serial dilutions from 900 nM to 0,14 nM and incubated at 37 °C. Three days later, the number of viable cells was evaluated using the CellTiter-Glo® Luminescent Cell Viability Assay (Promega). Luminescence values were measured using Victor Nivo 3F multiplate reader (PerkinElmer). Cell viability was analyzed with GraphPad software applying a curve fitting nonlinear regression model.

For the analysis of cellular substrate acetylation induced by treatment with compounds, 100.000 HeLa cells per well were seeded in 6-well plates one day before treatments. The day after, three serial dilutions of each compound were added to cells and incubated for 16 h at 37 °C. At the end of treatment cells were rinsed in PBS and lysed in 1% SDS in PBS for Western blot analysis of acetylated proteins.

A549 cell line (DMSZ) was cultured in Dulbecco's modified Eagle's medium (DMEM) (Euroclone, Italy) supplemented with 10% fetal bovine serum (FBS) (Sigma-Aldrich, Italy), 2 mM L-glutamine (Euroclone), and antibiotics (100 U/mL penicillin, 100 μg/mL streptomycin, and 250 ng mL^{-1} amphotericin-B; from Euroclone). Cells were treated with compounds for 24 h at 0.25, 1 and 10 μM. HeLa cells (ATCC) were grown in Dulbecco's modified Eagle's medium (DMEM) supplemented with 10% fetal bovine serum (FBS), 2 mM L-Glutamine and antibiotics (100 U/mL penicillin, 100 μg/mL streptomycin), all reagents by Euroclone.

1.5×10^6 cells were plated and after 24 h stimulated with candidate compounds at a concentration of 0.25, 1 and 10 μM.

2.4. Western blot analysis

A549 cells were lysed in RIPA buffer (1% Triton X-100, 0.1% SDS, 150 mM NaCl, 1 mM EDTA pH 8, 10 mM Tris-HCl pH 8) containing 1% protease inhibitor cocktail (Roche). Cell extract was sonicated for 5 min (30 s ON and 30 s OFF) and centrifuged for 15 min at 4 °C, the supernatant was then diluted 1:1 in sample buffer 2X Laemmli (0.217 M Tris-HCl pH 8.0, 52.17% SDS, 17.4% glycerol, 0.026% bromo-phenol blue, 8.7% beta-mercapto-ethanol) and subsequently boiled for 3 min; 15 μg of protein extract was subjected to SDS-polyacrylamide gel electrophoresis, then blotted on PVC membrane (Bio-Rad, USA) and incubated overnight with appropriate antibodies. Protein expression was detected by ECL Chemiluminescence method (Bio-Rad). Bands intensity was quantified by Image J analysis. Antibodies used for WB: anti-acetyl α-tubulin (cell signaling cat num #3971); anti-GADPH (Elabscience cat num #20059); anti-H4 (Elabscience cat num #65815) anti $H3K_{9,14}ac$ (diagenode cat num #15410005).

Total HeLa cell extracts were prepared with 1% SDS in PBS and quantified, then 5 μg per sample were analyzed by SDS-PAGE and Western Blot. After blocking with 5% non-fat milk, primary antibodies (anti-Acetyl-H3; anti-GAPDH; anti-Acetyl-alpha-Tubulin; Merck Millipore) were incubated overnight at 4 °C. HRP-conjugated secondary antibodies were incubated 40 min at room temperature and developed using a SuperSignal™ West Dura Extended Duration Substrate kit (Thermofisher Scientific). Chemiluminescence was revealed by means of a ChemiDoc Imaging System (Bio-Rad).

For Histone extraction: 5 × 106 cells were collected and washed two times with PBS and lysed in Tritonextraction buffer (TEB: PBS, 0.5% Triton X 100 (v/v), 2 mM PMSF, 0.02% (w/v) NaN3) for 10 min on ice, with gentle shaking and then centrifuged (2000 rpm at 4 °C for 10 min). Next, the supernatant was removed, and the pellet was washed in TEB and centrifuged as before. The pellet was resuspended in

0.2 N HCl and rotated overnight at 4 °C. The following day, the samples were then centrifuged at 2000 rpm for 10 min at 4 °C and the supernatant was collected.

2.5. Experimental mouse plasma determination of compound **2**

2.5.1. Chemicals and reagents

Methanol, acetonitrile, and other organic solvents were of chromatography grade from Sigma-Aldrich (Milano, Italy), water was purified using a milliQ system from Millipore (Billerica, MA, USA) and LC-MS grade formic acid was obtained from Fluka (Milano, Italy).

2.5.2. Stock solutions preparation

Compound **2** stock solution was prepared in DMSO at 1 mg/mL and stored at −20 °C. The stock solution was further diluted to obtain a working solution at 20 μg mL^{-1}. The modafienz drug was used as internal standard. Internal Standard Working Solutions (IS-WS) was prepared by adding appropriate volumes of the stock solution to 30 mL of 0.1% formic acid in methanol:acetonitrile (50:50, v/v), in order to reach a final concentration of 25 ng mL^{-1}. The solution was maintained at −20 °C.

2.5.3. Sample preparation

40 μL of rat plasma were mixed with 140 μL of IS-WS and 20 μL of 0.1% formic acid in methanol:acetonitrile (50:50, v/v). The mixture was vortex mixed for 1 min and centrifuged at 12,500 g for 10 min at 4 °C. The supernatant was collected and 8 μL were injected into the LC–MS/MS system.

2.5.4. LC-MS/MS analysis

Analysis was performed by liquid chromatography tandem mass spectrometry (LC–MS/MS). The HPLC equipment consists of an Exion LC AD System from AB Scienx (Toronto, ON, Canada). A 6500 QTRAP mass spectrometer from AB-Sciex (Toronto, ON, Canada) was used for detection. The analytes were analyzed using a Chromolith column (100 mm × 4.6 mm ID) from Merck KGaA. The mobile phases were (A) MeOH:AcN 50:50 and (B) water, both containing 0.05% formic acid, at a flow rate of 0.8 mL min^{-1} and were entirely transferred into the mass spectrometer source. The gradient elution was as follows: increase of the organic phase from 10 to 50% in 1.8 min, then to 100% in the following 0.4 min. Finally, after 1.3 min of 100% A the column was led to the original conditions in 2 min to enable equilibration of the column. Both the analyte and the IS were detected in negative ionization with a capillary voltage of −4500 V, nebulizer gas (air) at 50 psi, turbo gas (nitrogen) at 80 psi and 525 °C. The other ion source parameters were set as follows: curtain gas (CUR) 40 psi; collision gas (CAD) low; declustering potential (DP) −115 V, entrance potential (EP) −11 V.

Instrument conditions optimization was performed by direct infusion and manual tuning. Data collection and elaboration were performed by means of Analyst 1.7 software (AB- Sciex). The quantitative data were acquired using Multi Reaction Monitoring (MRM) mode. Two MRM transitions (precursor ion > fragment ion) were selected for the analytes. For compound **2** transitions were *m/z* 298.1. > 58.0 and 298.1 > 118.0, collision energy (CE) was set at −59 and −32 eV while collision cell exit potential (CXP) was at −24 and −15 V for the two transitions, respectively. For modafiendz the transitions were *m/z* 322.1. > 272.1 and 322.1 > 203.0, collision energy (CE) was set at −12 and −16 eV while collision cell exit potential (CXP) was at −28 and −15 V for the two transitions, respectively.

2.5.5. Method validation

The analytical method was validated according to FDA guidelines for bioanalytical method validation. Linearity, specificity, precision, accuracy, limits of detection (LODs) and lower limits of quantification (LLOQs) were evaluated. Calibration standard solutions were prepared in blank plasma by spiking 20 μL of a standard mixture at appropriate concentration to 40 μL of plasma and by adding 140 μL of methanol:acetonitrile (50:50, v/v). Calibrators were then treated similarly to the animal samples. The calibration range was 10–750 ng mL^{-1} and the calibrators were prepared at nine level of concentration. Precision, recovery and accuracy were evaluated at three level of concentrations (25, 100, 750 ng mL^{-1}) and resulted within the acceptable limits.

The limit of detection (LOD) was defined as the lowest concentration with a signal-to-noise (S/N) ratio greater than 3. The limit of quantification (LOQ) was defined as the concentration at which both precision (RSD %) and accuracy were less than 20%. LOQ resulted to be 10 ng mL^{-1} while LOD was 2 ng mL^{-1}.

2.6. Statistical analysis

Statistical analyses were performed with GraphPad Prism (GraphPad Software, Inc., San Diego, CA, USA) using a two-way ANOVA with Bonferroni's multiple comparison test for body weight changes and one-way ANOVA with Dunnett's multiple comparison test for the other readouts. Outlier data, identified by Grubbs' test, were excluded from the analysis. WB statistical analysis was performed by a two-tailed unpaired *t*-test. P-value (P) < 0.05 was considered significant. Experiments were performed in three biological replicates.

2.7. Ethics statements

Animal studies adhered strictly to the Italian Ministry of Health guidelines for the use and care of experimental animals. This study was performed according to protocols approved by the Institutional Animal Care and Use Committee (IACUC, protocol #733) of the San Raffaele Scientific Institute (Milan, Italy).

3. Results

3.1. Selection of HDAC6 inhibitors

To select a suitable compound for the *in vivo* PoC study a screening funnel was implemented on known (published and/or patented) HDAC6 inhibitors. Our first goal was the shortlisting of a small set of potent and selective known HDAC6 inhibitors. To this aim, we set an ideal threshold for HDAC6 potency (IC_{50} < 150 nM), selectivity (>100 over nuclear HDAC isoforms) and solubility features (>300 μM in a water/DMSO 96:4 system), while also paying attention to the synthetic feasibility for the selected compounds.

Upon analysis of scientific literature and relevant patents in the field (36 patents and 57 research articles), inhibitors **1** (Shen et al., 2016), **2** (Blackburn et al., 2013), and **3** (Song et al., 2015), (Fig. 1) were selected as the reference compounds to be putative candidate for the proof-of-concept study, taking into account HDAC6 inhibitory potency and selectivity profile over other HDAC isoforms as well as their synthetic feasibility. Moreover, one of our objectives was to test preclinical efficacy of selected HDAC6 inhibitor in mouse models of *P. aeruginosa* infection by aerosol administration. This route of administration requires formulation studies; in particular, it implies that the vehicle should be represented by an aqueous solution containing only a minimal percentage of organic solvents, such as dimethyl sulfoxide.

Accordingly, three short-listed compounds were identified from our analysis as the candidates more likely fitting to our established requirements with respect to HDAC6 potency/selectivity and solubility profile (Fig. 1). To compare these parameters in identical experimental conditions, compounds **1–3** were resynthesized and tested in an in-house panel of assays involving *in vitro* potency on HDAC6 over HDAC1 isoforms, and solubility profile. Solubility was determined for compounds **1** and **2**, since they displayed better selectivity. The in-house generated data are in line with those reported in the literature. Compound **2** dis-

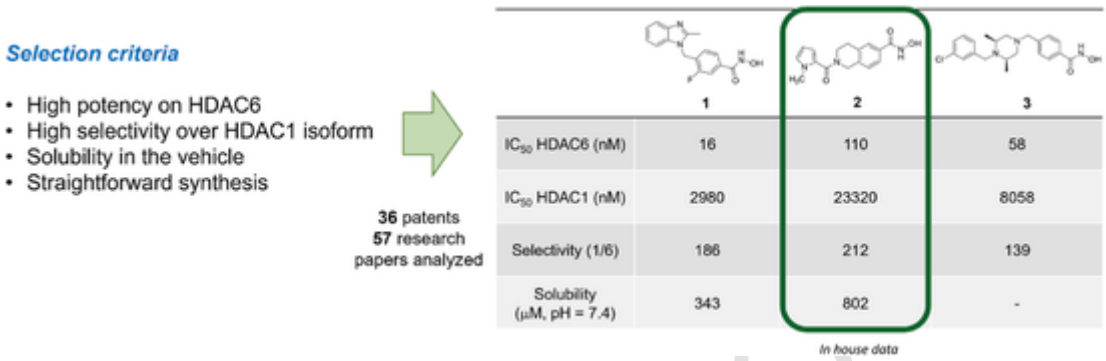

Fig. 1. Selective HDAC6 inhibitors selected as reference compounds. The values of IC_{50} on HDAC6 and HDAC1 and the solubility profiles are in house generated data. Detailed protocols are described in the materials and methods section.

played the best selectivity profile among the shortlisted compound and a significantly better solubility profile for compound **2** compared to inhibitor **1** (802 μM *vs* 343 μM at pH = 7.4), thus demonstrating to be the suitable compound for the selected administration route.

Additionally, the three selected compounds were engaged in cell-based assays (HeLa cells) and, by Western blot (WB) analysis, the protein levels of acetylated α-tubulin (substrate of HDAC6, cytoplasmic HDAC isoform) and acetylated histone H_3 (substrate of nuclear HDAC isoforms) were analyzed (Fig. 2). Specifically, HeLa cells were treated for 16 h, and the concentration of acetylated tubulin and acetylated H3 histone were evaluated by WB analysis as markers for selective activity on HDAC6 in comparison to nuclear HDAC isoforms. The activity of the compounds was compared with LAQ824 (Fuino et al., 2003; Kato et al., 2007), a potent pan-HDAC inhibitor, able to increase both the levels of acetylated histone and acetylated α-tubulin and with untreated cells (Ctrl). The selected compounds showed a significant increase in the levels of acetylated tubulin, but almost no effect on the acetylation of H3 at the tested concentrations, which indicates their selective action on HDAC6 enzyme. The dose-dependent activity also confirms the favorable cell penetration profile for the three selected inhibitors (see Fig. 3).

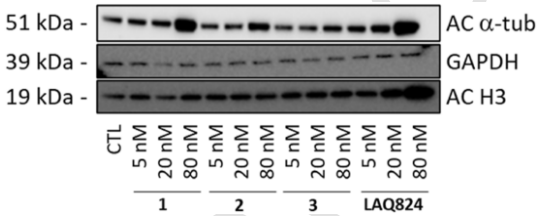

Fig. 2. Western Blot Analysis of acetylated α-tubulin (AC α-tub) and Histone H3 (AC H3) Expression Levels in HeLa Cells for compounds **1**, **2** and **3** compared with untreated control and LAQ824. The compounds were treated at the indicated concentrations for 16 h. Glyceraldehyde-3-phosphate dehydrogenase (GAPDH) was used as a loading control and negative control of acetylation.

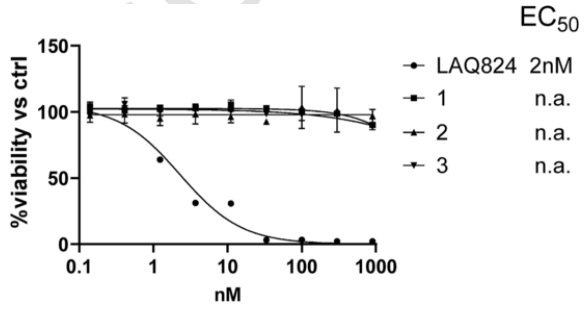

Fig. 3. Cytotoxicity of compounds **1–3**. EC_{50} was measured as cell viability of HeLa cells after 72 h incubation of a dose curve of compounds **1–3** in comparison with LAQ824.

Moreover, a cellular toxicity assay was performed on HeLa cells. The positive reference compound used in this cell-based assay was LAQ824, a potent pan HDAC inhibitor. HeLa cells were treated with a dose curve of compounds **1–3** and viability was assessed after 72 h Results are reported in.

While the reference compound LAQ824 showed an CC_{50} = 2 nM, all the HDAC6 selective compounds showed no significant toxicity. In particular, compound **2** did not display detectable toxicity at any concentration, not even at the maximum tested dose.

To explore in a lung cellular context the HDAC6 inhibitory potential of the selected compounds, we carried out a WB analysis assaying acetylation levels of α-tubulin (ac-tub), a specific target of HDAC6, and $H3K_{9,14}Ac$. A549 lung cancer cells were treated with compounds **1–3** at 0.25, 1 and 10 μM (Fig. 4). Interestingly, we observed that all analyzed compounds, although to a different extent, were able to increase protein levels of ac-tub in a dose-dependent manner. Conversely, a slight increase of $H3K_{9,14}Ac$ levels was only observed following treatments at 10 μM for compound **1**, and no $H3K_{9,14}Ac$ upregulation was found for the other compounds analyzed, indicating that the analyzed compounds are specific for HDAC6 compared to other HDAC isoforms.

Taking into account all the data generated in house, we selected compound **2** as the best performing candidate to be engaged in efficacy mouse model PoC studies that included three different *in vivo* studies, namely i) the assessment of acute toxicity of compound **2** at different doses and the selected vehicle, ii) the efficacy in a mouse model of *P. aeruginosa* acute lung infection, and iii) the efficacy in a mouse model of *P. aeruginosa* chronic lung infection (PoC experiment).

*3.2. Toxicity and efficacy of compound **2** in mouse model of P. aeruginosa acute and chronic respiratory infection*

Acute toxicity studies showed that mice treated twice with three doses of compound **2** (5, 10 and 20 mg/kg) did not show weight loss and temperature decrease or other evident effects on health status (data not shown) compared to vehicle-treated mice (PBS + 4% DMSO). The positive outcome of the acute toxicity experiment supported the feasibility of *in vivo* efficacy assessment of compound **2** at the three selected doses.

The efficacy of compound **2** was evaluated in a mouse model of *P. aeruginosa* acute respiratory infection. C57BL/6NCrl mice were challenged with planktonic *P. aeruginosa* PAO1 strain by i.t. inoculation to induce acute infection. Aerosol treatment with compound **2** at 5, 10 and 20 mg/kg or vehicle (PBS + 4% DMSO) started 18 h before and 5 min after infection. A single dose of compound **2** at 5 and 10 mg/kg showed a trend in bacterial load reduction, both in the lung and in the BALF, but this difference was not statistically significant (Fig. 5A). Moreover, no effect on cell recruitment was shown after treatment with compound **2** (Fig. 5B). These results suggest that a single dose of **2** by

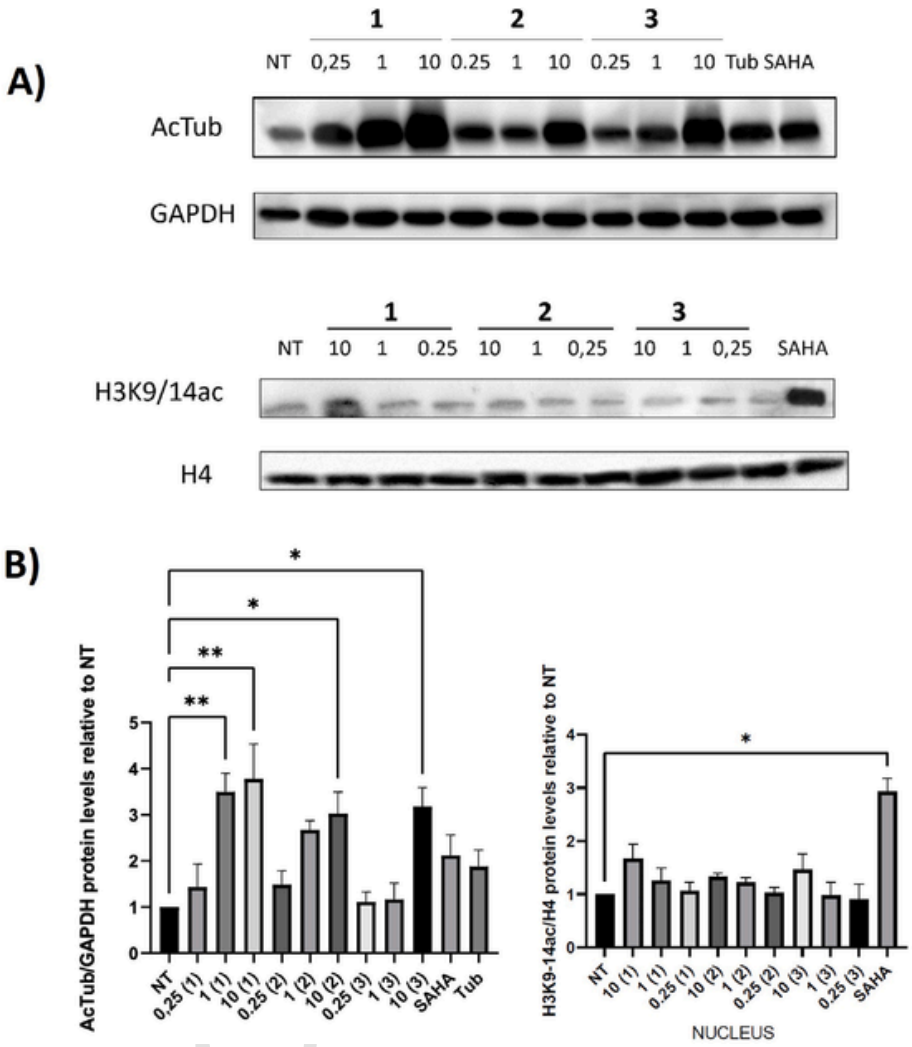

Fig. 4. A) Western Blot analysis showing protein expression levels of acetylated α-tubulin (AcTub) and acetylated histone 3 (H3K9/14ac) following 24 h treatment with the indicated compounds (**1**, **2** and **3**) at indicated concentrations (10, 1 and 0.25 μM). SAHA was used as a positive control. GADPH and H4 were used as a Western Blot loading control. B) Densitometric analysis of WB. Errors bars indicate the standard deviation of three biological replicates, n = 3 (**$P < 0.01$; *$P < 0.05$).

aerosol is not effective in ameliorating inflammation and infection in a mouse model of *P. aeruginosa* acute infection.

The results obtained in the *P. aeruginosa* acute infection model were not surprising due to the short time window explored, probably too short to see any effect based on the epigenetic mechanism of the HDAC6 inhibition. We envisaged more appropriate experimental conditions, thus planned to test the efficacy of **2** in a chronic lung infection model, also supported by literature data highlighting that genetic depletion of HDAC6 improved both the inflammatory state and the infection in chronically infected mice with *P. aeruginosa* (Rosenjack et al., 2019).

To mimic a chronic infection similar to what is typically established in the lungs of CF patients, mice received intratracheal inoculations of 4–5x10^5 *P. aeruginosa* MDR-RP73 strain embedded in agar beads.[18] Five minutes after infection mice were treated aerosol by Penn Century with compound **2** at 5, 10 and 20 mg/kg or vehicle (PBS + 4% DMSO). Mice were treated daily for three or seven days and sacrificed at two different time points (Fig. S1) (Bragonzi, 2010; Bragonzi et al., 2005). Body weight recovery did not differ between compound **2** and vehicle-treated mice after infection (Fig. 6A). Three treatments with compound **2** induced reduction in bacterial load, although not statistically significant (Fig. 6B). At this early time point we observed no efficacy of compound **2** in reducing cell recruitment (Fig. 6C).

Next, when we extended the treatment to 7 days, compound **2**-treated mice exhibited less loss and faster recovery of body weight in dose dependent manner than vehicle-treated mice (Fig. 7A). We observed a relevant efficacy in bacterial load reduction after treatment with compound **2**, but this effect was not statistically significant (Fig. 7B).

To define the effect of repeated treatments on the airway inflammatory response, total leukocyte recruitment in the BALF was evaluated. After 7 days of treatment, mice treated with the inhibitor showed a dose-dependent reduction in total cell counts and in the number of neutrophils in BALF that was significant at the doses 10 and 20 mg/kg (Fig. 7C) as compared to vehicle-treated mice.

Statistical significance determined by one-way ANOVA followed by Dunnett's Multiple Comparison Test: *P < 0.05, **P < 0,01 HDAC6i-treated mice compared to vehicle treated mice.

Following the significant anti-inflammatory efficacy of compound **2** at 10 mg/kg and 20 mg/kg we evaluated the effect of treatment on chemokines and cytokines assay on the supernatant of lung homogenates. Treatment with the highest dose of compound **2** induced a statistically significant reduction of several interleukins involved in the inflammatory response (IL-1α, IL-1β, IL-4, IL-6, IL-9, IL12 (p70) and IL-17A), chemokines (KC, MCP-1, MIP-1α, MIP-1β and RANTES), growth

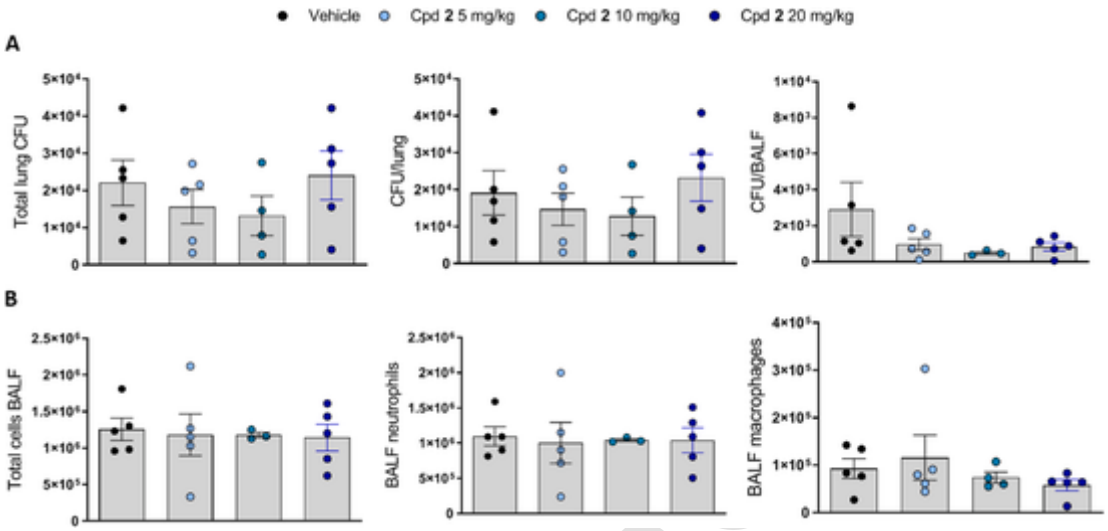

Fig. 5. Efficacy of compound **2** (Cpd **2**) at 5 mg/kg, 10 mg/kg, 20 mg/kg aerosol treatment in *P. aeruginosa* PAO1 acute infection model; bacterial load count, including lung and BALF (A) and cellular recruitment, including neutrophils and macrophages after compound treatment in comparison with vehicle (B). Data are presented as mean ± SEM.

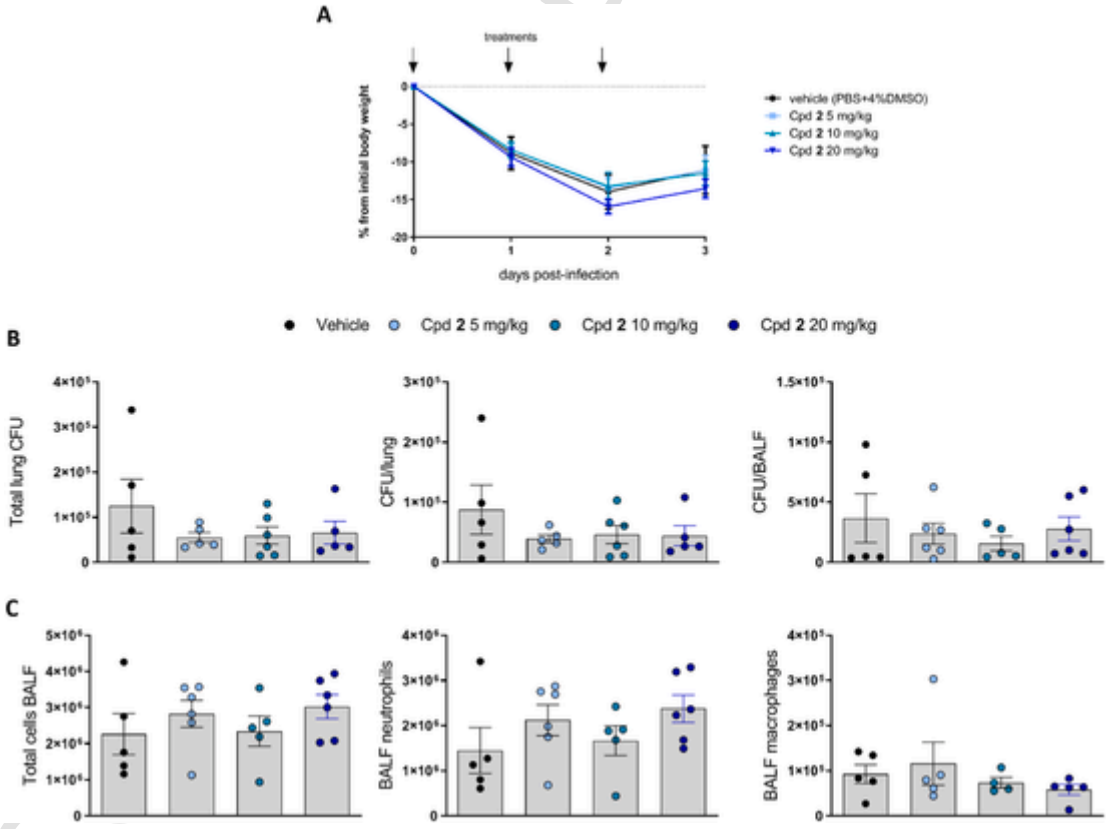

Fig. 6. Efficacy of compound **2** (Cpd **2**) at 5 mg/kg, 10 mg/kg, 20 mg/kg aerosol treatment in *P. aeruginosa* MDR-RP73 three days chronic infection model; body weight evaluation (A), bacterial load count in the lung, including lung and BALF (B) and cellular recruitment (C), including neutrophils and macrophages after compound **2** treatment in comparison with vehicle. Data are presented as mean ± SEM.

factors (G-CSF) and IFN-γ when compared with vehicle-treated mice (Fig. 8).

Overall, these data confirm the capacity of the compound **2** in reducing inflammation induced by *P. aeruginosa* chronic lung infection.

Statistical significance determined by one-way ANOVA followed by Dunnett's Multiple Comparison Test: *P < 0.05, **P < 0,01, ***P < 0,001, ****p < 0,0001 HDAC6i-treated mice compared to vehicle treated mice.

*3.3. Biodistribution studies on compound **2** demonstrates negligible plasma concentration upon intratracheal administration*

Plasma samples collected from chronic infection mice treated with compound **2** were submitted to quantitative determination of the compound in this biological matrix (See Materials and Methods section for details) in order to assess the circulating plasma concentration after 3 and 7-days treatment by intratracheal injection. The evaluation of this

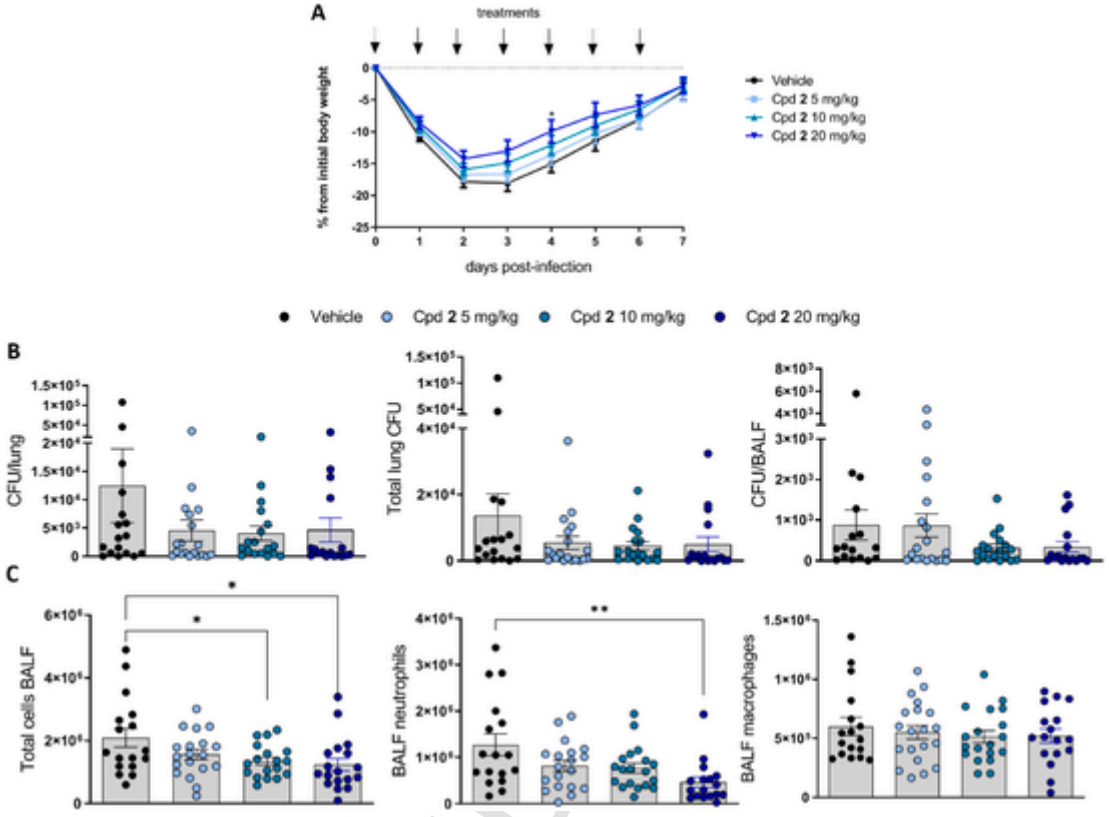

Fig. 7. Efficacy of compound **2** (Cpd **2**) at 5 mg/kg, 10 mg/kg, 20 mg/kg aerosol treatment in *P. aeruginosa* MDR-RP73 seven days chronic infection model; body weight evaluation (A), bacterial load count (B) and cellular recruitment after Cpd **2** or vehicle treatment. Data are presented as mean ± SEM pooled from three experiments.

parameter is essential to understand the body distribution of the compound after aerosol administration and the suitability of our conceived formulation for a potential chronic use. In general, intratracheal administration did not induce massive systemic circulation and our data confirm the general trend also for compound **2**. The quantitative evaluation demonstrated that the compound is not distributed in the body even after a 7 days QD treatment (Table 1): in most samples the target compound was not detected, in some samples the peak was visible but under the limit of quantification (<10 ng mL^{-1}) while only in a few cases quantification could be carried on. The maximum detected concentration was 21 ng mL^{-1}, which can be considered a negligible concentration. These findings support the safe profile of **2** in our administration settings.

These data prove that compound **2** is localized only at the site of administration (lung) where it can carry out the positive effect against inflammation and bacterial load.

4. Discussion

Developing new therapeutic options for CF is closely linked to the necessity of identifying novel treatment approaches, which could allow the resolution of the prolonged and aggressive inflammatory phenotype associated to CF, but also guarantee sustained immune response for the eradication on infections that are one of the leading causes of complications and death of the patients.

The goal of this study is providing a solid proof of concept for HDAC6 selective inhibitors to reduce the inflammatory status and infection in validated *P. aeruginosa* acute and chronic infection models.

Clear evidence has been provided in the last years that host protein acetylation status is dynamically regulated during infection and correlated to the modulated immune response against pathogens. Recent data also highlighted the role of microtubule acetylation as a key regulator of intracellular transport in CF cells and CF-related inflammatory responses. In this context HDAC6, owing to its distinctive structure, localization and nature of substrates, plays a pivotal role in the acetylation-deacetylation balance of key protein substrates, thus supporting the concept that several CF phenotypes can be ameliorated through HDAC6 inhibition.

The microtubule network undergoes extensive post-translational modifications (PTMs), including acetylation. PTMs are largely responsible for the fine-tuning of microtubule network stability, as well as the recruitment of microtubule-associating proteins (Song et al., 2015; Westermann and Weber, 2003; Wloga et al., 2017; Moutin et al., 2021). α-Tubulin was the first acknowledged HDAC6 protein substrate. Accordingly, increased expression of HDAC6 promotes tubulin hypoacetylation, thus controlling chemotactic cell movement (Hubbert et al., 2002; Cabrero et al., 2006; Haggarty et al., 2003) and motor-based trafficking (Kawaguchi et al., 2003).

Multiple evidences also supported the hypothesis that the microtubule acetylation status is responsible for the defective endocytic trafficking and perinuclear cholesterol accumulation detected in CF (Rymut et al., 2013, 2017).

Tubastatin A (TubA), a selective HDAC6 inhibitor, was employed as a pharmacological tool and helped unveiling the effectiveness of HDAC6 inhibition in cell-based models in increasing the levels of Ac-tubulin and relocating of accumulated perinuclear cholesterol (Rymut et al., 2013; Lu et al., 2019), thus demonstrating that tubulin acetylation is a crucial pathway in pathophysiology of several CF phenotypes and that HDAC6 inhibition holds promising potential as innovative therapeutic option for restoring those pathways to a more WT-like pattern.

The evidence of a dynamic regulation of epigenetic marks by environmental cues has also triggered research efforts devoted to the eluci-

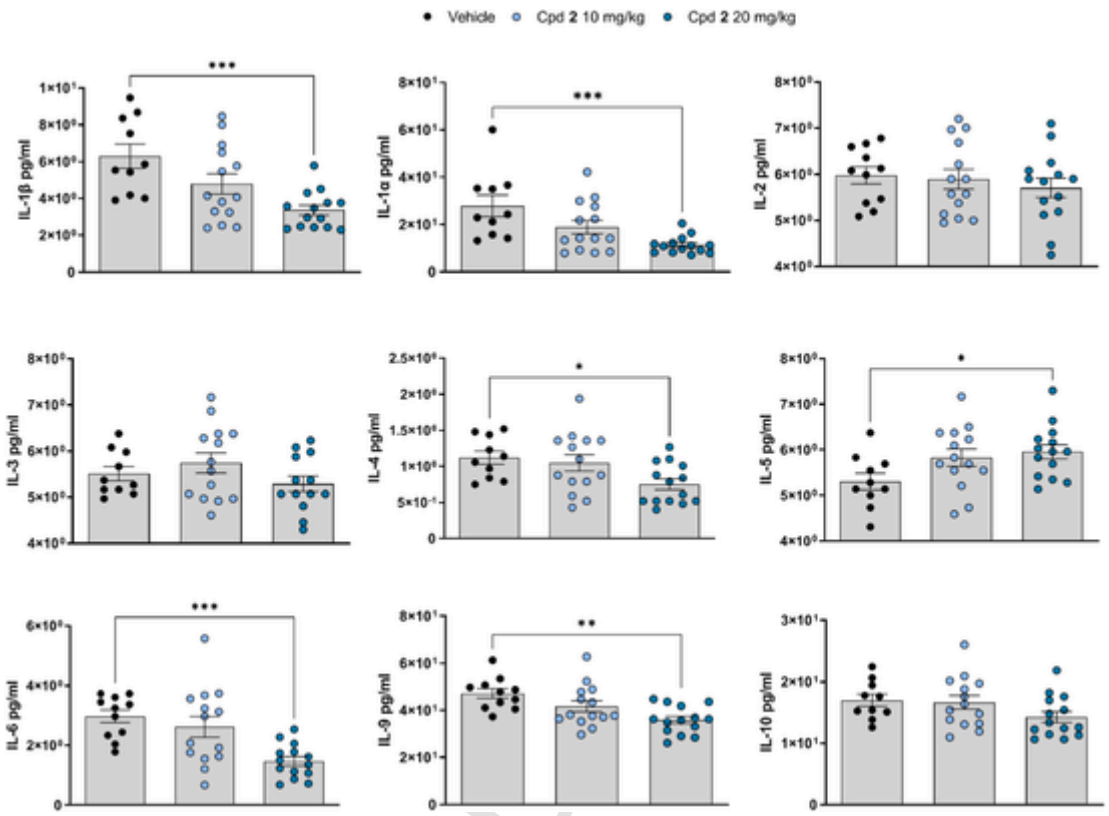

(*caption on next page*)

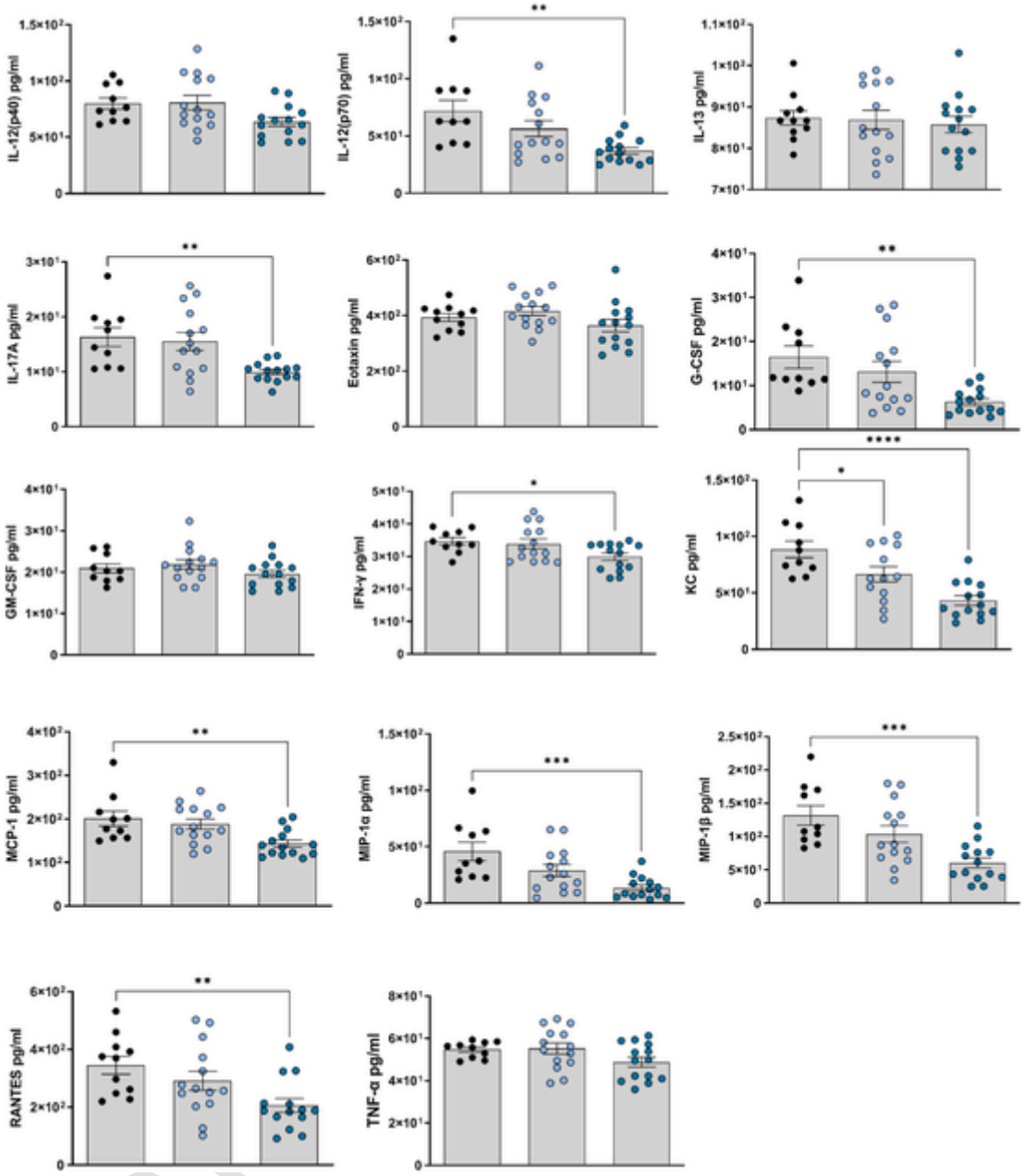

Fig. 8. Bioplex immunoassays results evaluated in supernatant of lung homogenates after compound **2** (Cpd **2**) at 10 mg/kg and 20 mg/kg or vehicle aerosol treatment in *P. aeruginosa* MDR-RP73 seven days chronic infection model. Data shown were pooled from three experiments performed in different days.

Table 1
Compound **2** quantification in plasma samples.

Dose	Days post infection	Concentration range (n = 6)
5 mg/kg	3	ND to 20 ng mL^{-1}
10 mg/kg	3	ND to 21 ng mL^{-1}
20 mg/kg	3	ND to 14 ng mL^{-1}
5 mg/kg	7	ND
10 mg/kg	7	ND
20 mg/kg	7	ND

*ND: Not Detected.

dation of epigenetic pathways in microbial infections (Grabiec and Potempa, 2018; Correa-Oliveira et al., 2016; Beier et al., 2012).

Interestingly, it was demonstrated that TubA, but not class I HDAC inhibitors, enhanced bacterial killing by macrophages (Ariffin et al., 2015). The same study also evidenced that treatment with HDAC inhibitors at the insurgence of bacterial infection boosts mitochondrial reactive oxygen species production by human macrophages, thus in turn increasing antibacterial response. Almost parallel studies also demonstrated that HDAC6 selective inhibition promoted bacterial clearance, reduced pro-inflammatory cytokine production, restored innate immune cell populations in the bone marrow, and improved survival in a mouse model of sepsis (Li et al., 2015; Zhao et al., 2016). These data support the hypothesis of a key role for HDAC6 in regulating bacterial clearance (Chen et al., 2008; Kamemura et al., 2012; Bai et al., 2015), while class I HDACs seem unlikely to exert such effect.

These data were also validated by genetic *Hdac6* depletion, demonstrating reduced bacterial load in a model of infection using clinical *P. aeruginosa* isolates embedded in agarose beads, which effectively recapitulates CF phenotype (Rosenjack et al., 2019). These data, coupled with the limited weight loss registered and the regulation of neutrophil recruitment upon *Hdac6* depletion, further highlight HDAC6 as a crucial regulator in multiple secondary phenotypes related to impaired

CFTR function, thus supporting the use of selective HDAC6 inhibitors in CF patients regardless of CFTR phenotype.

Fully, in line with these results we have herein demonstrated that selective pharmacological HDAC6 blockade with compound **2** can exert significant effects on infection in an *in vivo* mouse model of chronic *PA* infection.

In particular, treatment of mice with aerosol by Penn Century with compound **2** at the three selected doses (5 mg/kg, 10 mg/kg and 20 mg/kg daily for a total of seven administrations) led to a strong reduction of infection at all doses, measured as a reduction of bacterial load (CFU count).

In the context of inflammation, increasing evidence is available highlighting the key role of HDACs and HDAC inhibitors in the regulation of chemokines, cytokines and growth factors, thus controlling key inflammatory pathways in inflammatory diseases of different origins (Gatla et al., 2019; Bolden et al., 2013; Hull et al., 2016; Nusinzon and Horvath, 2003; Vlasakova et al., 2007; Deng et al., 2018). In particular, a predominant role of HDAC6 isoform on the regulation of cytokines levels has been highlighted by several reports. Accordingly, HDAC6 selective inhibition was shown to down-regulate IL-1β expression in fibroblasts, epithelial and myogenic cell lines (Di Liddo et al., 2016); moreover, the pivotal role of HDAC6 in the regulation of NF-kB activity, related to IL-1β signaling was disclosed (Cheng et al., 2014a,b). Selective HDAC6 inhibition was also linked to reduction of IL-6 in an arthritis mouse model (Vishwakarma et al., 2013), while the role of this isoform on the production of the anti-inflammatory cytokine IL-10 is still controversial (Di Liddo et al., 2016; Licciardi and Karagiannis, 2012).

HDAC involvement in chemokine signaling was also demonstrated; accordingly, pan-HDAC inhibition induced the expression of CCL2 (Booth et al., 2017), and selective HDAC6 inhibition decreased CCL4 expression (Choi et al., 2018; Cao et al., 2018).

HDAC6 also appears an important player in the regulation of inflammatory cells. In particular, HDAC6 inhibition stimulates inflammatory antigen-presenting cells with a key role in the induction of T-cell activation and T-cell tolerance (Cheng et al., 2014a,b; Yan et al., 2017; Cheng et al., 2014a,b). Moreover, depletion of HDAC6 endorses the suppressive activity of Foxp3$^+$ regulatory T-cells in inflammation models (de Zoeten et al., 2011).

According to this data, targeted HDAC6 inhibition has been increasingly proposed over the last years as a promising therapeutic strategy towards inflammatory disorders, including airway inflammation (Ran and Zhou, 2019), asthma (Ren et al., 2016), and chronic obstructive pulmonary disease (COPD) (Lam et al., 2013).

In the context of CF, inflammation-oriented studies evaluated the effect of pan-HDAC inhibition in *P. aeruginosa*-lipopolysaccharides (*PA*-LPS)-induced airway inflammation and CF lung disease (Bodas et al., 2018). In this model, pan-HDAC inhibition efficiently controlled *P. aeruginosa*-LPS-induced IL-6 levels. Moreover, the same study demonstrated that NF-kB activation (as a marker of inflammation) and Nrf2 regulation (as a marker of anti-oxidant response) are effectively corrected by pan-HDAC inhibitors (Bodas et al., 2018). More recent evidence pointed out the unique role of HDAC6 isoform with respect to the inflammatory phenotype in CF, thus supporting the evaluation of selective HDAC6 inhibitors in this context. Accordingly, it was recently demonstrated that HDAC6 genetic depletion improved CF mouse airway inflammatory responses to bacterial challenge, in a clinical *P. aeruginosa* chronic infection model (Rosenjack et al., 2019). Additionally, the loss of *Hdac6* on a CF background increased the rate of bacterial clearance, and this effect was ascribed to a crucial regulatory step in CF immune responses.

Here, we tested HDAC6 selective inhibitors in validated *P. aeruginosa* mouse models that recapitulate the bacterial infection and the inflammation status in the early and late CF disease (Bragonzi, 2010). In particular, the pre-clinical testing of compound **2** was performed in acute infection and complex models of long-term chronic airway infection by challenging mice with the MDR-RP73 *P. aeruginosa* clinical strain embedded in agar beads. We have previously shown that agar beads provide micro-anaerobic conditions for bacterial growth and biofilm formation comparable to those present in the mucus of CF patients (Bragonzi et al., 2005; Worlitzsch et al., 2002; Cigana et al., 2016). In addition, this model develops lesions similar to the ones found in CF patients and displays certain phenotypes of human CF lung disease, providing a valuable tool for the pre-clinical testing of antibacterial and anti-inflammatory molecules (Döring et al., 2014; De Leo et al., 2022). Fully, in line with *in vitro* results we demonstrated that selective pharmacological HDAC6 blockade can exert significant effects in the regulation of inflammatory markers in an *in vivo* mouse model of chronic *P. aeruginosa* infection. In particular, treatment of mice with aerosol by Penn Century with compound **2** at three doses by applying repeated administrations led to a significant anti-inflammatory effect, causing a dose-dependent reduction in total cell counts and in the number of neutrophils in BALF. Furthermore, the anti-inflammatory effect of compound **2** was confirmed by Bio-plex Multiplex immunoassay, where treatment with the highest dose induces a statistically significant reduction of key interleukins involved in the inflammatory response. Most important, considering the potential interference of compound **2** with innate immune recruitment mechanisms, we evaluated the possible risk of favoring bacterial infections. In the chronic infection model, compound **2** efficacy was associated with a modest decrease of bacterial burden, indicating no risk of pulmonary exacerbation in repeated treatments. Thus, this anti-inflammatory activity is accompanied by a beneficial protecting activity against infection. Although our study represents the first proof of concept for efficacy of pharmacological HDAC6 blockade in mouse models of chronic *P. aeruginosa* infection, the challenge ahead is to improve these mouse models by including additional variables such as the CFTR mutations and the concomitant use of other therapies to further reflect the complexity of CF disease.

In summary, we herein provided the first comprehensive *in vivo* proof-of concept of the efficacy of a selective HDAC6 inhibitor in contrasting the CF-associated proinflammatory phenotype as well as in effectively reducing bacterial load in treated animals. After a careful compound selection performed based on HDAC6 potency and selectivity, we identified compound **2** as the most suitable candidate to be engaged in *in vivo* studies for validating our hypothesis.

We re-profiled compound **2** in house on its HDAC1/6 inhibitory activity and assessed its performance in selectively increasing levels of acetylated tubulin with respect to acetylated histone levels in HeLa and A549 cells. The behaviour of compound **2** in cell-based settings demonstrated its striking preference for the inhibition of HDAC6 with respect to nuclear HDAC isoforms, thus further supporting its favorable features as optimum chemical probe to specifically dissect the role of selective HDAC6 inhibition as innovative therapeutic option in CF. As a further validation of its drug-like profile, compound **2** did not cause toxic effects in cells, neither it caused weight loss, temperature decrease or any other evident effects on health status of treated mice. We showed that **2** is able to dose-dependently reduce the total cell counts and neutrophils in BALF and evoke a modest reduction of the bacterial load, when locally administered in a mouse model of chronic *Pseudomonas aeruginosa* infection using a Penn-Century MicroSprayer® Aerosoliser. The anti-inflammatory profile of **2** has been further validated by bioplex analysis, which highlighted significant changes in the level of interleukins and other relevant inflammatory markers, thus unequivocally validating selective HDAC6 inhibition as a feasible strategy for reducing inflammation and bacterial load related to CF phenotype.

Our study is of particular significance since it demonstrates for the first time the utility of selective drug-like HDAC6 inhibitors as innovative therapeutic option for CF, using a relevant *in vivo* model. Our data pave the way to the development of novel HDAC6 inhibitors specifically tailored for chronic administration in CF patients, thus improving

the CF-associated inflammatory phenotype and promoting an effective immune response against infections.

Authorship contribution statement

Conceptualization, design and manuscript writing: M.B and V.S.; Chemical synthesis and scale-up of HDAC6 inhibitors: S.B., E.C. and A.A; Development of methodology: G.F.; Acquisition of data: G. F. and A.J.F.M., Analysis and interpretation of data (e.g., statistical analysis, biostatistics, computational analysis): G.F., A.J.F.M.; Cell-based assays: G. B and Me.Ba.; Design of biological cell-based studies: N.D.G. and L.A.; Design of the *in vivo* experiments: A.B and A.R.; *in vivo* experiments: A.R., D.G. and I.DF.; Data analysis: A.R., A.B., D.G.; Manuscript editing: G.F., A.B., A.R., I.DF and D.G.; Biodistribution study: C.M. and M.C.

Declaration of competing interest

The Authors declare no competing interest.

Uncited References

Bodas and Vij, 2010; Song and Brady, 2015.

Data availability

Data will be made available on request.

Acknowledgements

The authors thank Fondazione Fibrosi Cistica (FFC) for financial support through Grant FFC#20/2020: Harnessing selective histone deacetylase 6 (HDAC6) inhibition to tackle inflammation and fibrotic remodeling in cystic fibrosis. M.B., V.S., S.B, E.C and A.A also acknowledge MIUR Grant Dipartimento di Eccellenza 2018–2022 (l. 232/2016) to the Department of Pharmacy, University of Naples Federico II. The authors thank VALERE: Vanvitelli per la Ricerca Program: EPInhibit-DRUGre (CUP B66J20000680005) and the MISE: Nabucco Project. N.D.G. was supported by PON Ricerca e Innovazione 2014–2020- Linea 1, AIM - AIM1859703.

Appendix A. Supplementary data

Supplementary data to this article can be found online at https://doi.org/10.1016/j.ejphar.2022.175349.

References

Ariffin, J.K., das Gupta, K., Kapetanovic, R., Iyer, A., Reid, R.C., Fairlie, D.P., Sweet, M.J., 2015. Histone deacetylase inhibitors promote mitochondrial reactive oxygen species production and bacterial clearance by human macrophages. Antimicrob. Agents Chemother. 60, 1521–1529.

Bai, J., Lei, Y., An, G.L., He, L., 2015. Down-regulation of deacetylase HDAC6 inhibits the melanoma cell line A375.S2 growth through ROS-dependent mitochondrial pathway. PLoS One 10, e0121247.

Beier, U.H., Wang, L., Han, R., Akimova, T., Liu, Y., Hancock, W.W., 2012. Histone deacetylases 6 and 9 and sirtuin-1 control Foxp3+ regulatory T cell function through shared and isoform-specific mechanisms. Sci. Signal. 5, ra45.

Blackburn, C., Barrett, C., Chin, J., Garcia, K., Gigstad, K., Gould, A., Gutierrez, J., Harrison, S., Hoar, K., Lynch, C., Rowland, R.S., Tsu, C., Ringeling, J., Xu, H., 2013. Potent histone deacetylase inhibitors derived from 4-(aminomethyl)-N-hydroxybenzamide with high selectivity for the HDAC6 isoform. J. Med. Chem. 56, 7201–7211.

Bodas, M., Vij, N., 2010. The NF-kappaB signaling in cystic fibrosis lung disease: pathophysiology and therapeutic potential. Discov. Med. 9, 346–356.

Bodas, M., Mazur, S., Min, T., Vij, N., 2018. Inhibition of histone-deacetylase activity rescues inflammatory cystic fibrosis lung disease by modulating innate and adaptive immune responses. Respir. Res. 19, 2.

Bolden, J.E., Shi, W., Jankowski, K., Kan, C.Y., Cluse, L., Martin, B.P., MacKenzie, K.L., Smyth, G.K., Johnstone, R.W., 2013. HDAC inhibitors induce tumor-cell-selective pro-apoptotic transcriptional responses. Cell Death Dis. 4, e519.

Booth, L., Roberts, J.L., Poklepovic, A., Kirkwood, J., Dent, P., 2017. HDAC inhibitors enhance the immunotherapy response of melanoma cells. Oncotarget 8, 83155–83170.

Boucher, R.C., 2004. Relationship of airway epithelial ion transport to chronic bronchitis. Proc. Am. Thorac. Soc. 1, 66–70.

Bragonzi, A., Worlitzsch, D., Pier, G.B., Timpert, P., Ulrich, M., Hentzer, M., Andersen, J.B., Givskov, M., Conese, M., Doring, G., 2005. Nonmucoid Pseudomonas aeruginosa expresses alginate in the lungs of patients with cystic fibrosis and in a mouse model. J. Infect. Dis. 192, 410–419.

Bragonzi, A., 2010. Murine models of acute and chronic lung infection with cystic fibrosis pathogens. Int. J. Med. Microbiol. 300, 584–593.

Brindisi, M., Saraswati, A.P., Brogi, S., Gemma, S., Butini, S., Campiani, G., 2020. Old but gold: tracking the new guise of histone deacetylase 6 (HDAC6) enzyme as a biomarker and therapeutic target in rare diseases. J. Med. Chem. 63, 23–39.

Brindisi, M., Senger, J., Cavella, C., Grillo, A., Chemi, G., Gemma, S., Cucinella, D.M., Lamponi, S., Sarno, F., Iside, C., Nebbioso, A., Novellino, E., Shaik, T.B., Romier, C., Herp, D., Jung, M., Butini, S., Campiani, G., Altucci, L., Brogi, S., 2018. Novel spiroindoline HDAC inhibitors: synthesis, molecular modelling and biological studies. Eur. J. Med. Chem. 157, 127–138.

Bye, M.R., Ewig, J.M., Quittell, L.M., 1994. Cystic fibrosis. Lung 172, 251–270.

Cabrero, J.R., Serrador, J.M., Barreiro, O., Mittelbrunn, M., Naranjo-Suarez, S., Martin-Cofreces, N., Vicente-Manzanares, M., Mazitschek, R., Bradner, J.E., Avila, J., Valenzuela-Fernandez, A., Sanchez-Madrid, F., 2006. Lymphocyte chemotaxis is regulated by histone deacetylase 6, independently of its deacetylase activity. Mol. Biol. Cell 17, 3435–3445.

Cao, T., Zhou, X., Zheng, X., Cui, Y., Tsien, J.Z., Li, C., Wang, H., 2018. Histone deacetylase inhibitor alleviates the neurodegenerative phenotypes and histone dysregulation in presenilins-deficient mice. Front. Aging Neurosci. 10, 137.

Castellani, C., Assael, B.M., 2017. Cystic fibrosis: a clinical view. Cell. Mol. Life Sci. 74, 129–140.

Chen, J., Shi, X., Padmanabhan, R., Wang, Q., Wu, Z., Stevenson, S.C., Hild, M., Garza, D., Li, H., 2008. Identification of novel modulators of mitochondrial function by a genome-wide RNAi screen in Drosophila melanogaster. Genome Res. 18, 123–136.

Cheng, F., Lienlaf, M., Wang, H.W., Perez-Villarroel, P., Lee, C., Woan, K., Rock-Klotz, J., Sahakian, E., Woods, D., Pinilla-Ibarz, J., Kalin, J., Tao, J., Hancock, W., Kozikowski, A., Seto, E., Villagra, A., Sotomayor, E.M., 2014a. A novel role for histone deacetylase 6 in the regulation of the tolerogenic STAT3/IL-10 pathway in APCs. J. Immunol. 193, 2850–2862.

Cheng, F., Lienlaf, M., Perez-Villarroel, P., Wang, H.W., Lee, C., Woan, K., Woods, D., Knox, T., Bergman, J., Pinilla-Ibarz, J., Kozikowski, A., Seto, E., Sotomayor, E.M., Villagra, A., 2014b. Divergent roles of histone deacetylase 6 (HDAC6) and histone deacetylase 11 (HDAC11) on the transcriptional regulation of IL10 in antigen presenting cells. Mol. Immunol. 60, 44–53.

Choi, E.W., Song, J.W., Ha, N., Choi, Y.I., Kim, S., 2018. CKD-506, a novel HDAC6-selective inhibitor, improves renal outcomes and survival in a mouse model of systemic lupus erythematosus. Sci. Rep. 8, 17297.

Cigana, C., Lore, N.I., Riva, C., De Fino, I., Spagnuolo, L., Sipione, B., Rossi, G., Nonis, A., Cabrini, G., Bragonzi, A., 2016. Tracking the immunopathological response to Pseudomonas aeruginosa during respiratory infections. Sci. Rep. 6, 21465.

Correa-Oliveira, R., Fachi, J.L., Vieira, A., Sato, F.T., Vinolo, M.A., 2016. Regulation of immune cell function by short-chain fatty acids. Clin. Transl. Immunol. 5, e73.

De Leo, F., Rossi, A., De Marchis, F., Cigana, C., Melessike, M., Quilici, G., De Fino, I., Mantonico, M.V., Fabris, C., Bragonzi, A., Bianchi, M.E., Musco, G., 2022. Pamoic acid is an inhibitor of HMGB1·CXCL12 elicited chemotaxis and reduces inflammation in murine models of Pseudomonas aeruginosa pneumonia. Mol. Med. 28, 108.

Deng, R., Zhang, P., Liu, W., Zeng, X., Ma, X., Shi, L., Wang, T., Yin, Y., Chang, W., Zhang, P., Wang, G., Tao, K., 2018. HDAC is indispensable for IFN-gamma-induced B7-H1 expression in gastric cancer. Clin. Epigenet. 10, 153.

de Zoeten, E.F., Wang, L., Butler, K., Beier, U.H., Akimova, T., Sai, H., Bradner, J.E., Mazitschek, R., Kozikowski, A.P., Matthias, P., Hancock, W.W., 2011. Histone deacetylase 6 and heat shock protein 90 control the functions of Foxp3(+) T-regulatory cells. Mol. Cell Biol. 31, 2066–2078.

Di Liddo, R., Valente, S., Taurone, S., Zwergel, C., Marrocco, B., Turchetta, R., Conconi, M.T., Scarpa, C., Bertalot, T., Schrenk, S., Mai, A., Artico, M., 2016. Histone deacetylase inhibitors restore IL-10 expression in lipopolysaccharide-induced cell inflammation and reduce IL-1beta and IL-6 production in breast silicone implant in C57BL/6J wild-type murine model. Autoimmunity 1–11.

Döring, G., Bragonzi, A., Paroni, M., Akturk, F.F., Cigana, C., Schmidt, A., Gilpin, D., Heyder, S., Born, T., Smaczny, C., Kohlhaufl, M., Wagner, T.O., Loebinger, M.R., Bilton, D., Tunney, M.M., Elborn, J.S., Pier, G.B., Konstan, M.W., Ulrich, M., 2014. BIIL 284 reduces neutrophil numbers but increases P. aeruginosa bacteremia and inflammation in mouse lungs. J. Cyst. Fibros. 13, 156–163.

Facchini, M., De Fino, I., Riva, C., Bragonzi, A., 2014. Long term chronic Pseudomonas aeruginosa airway infection in mice. Jove-J. Vis. Exp. 85, 51019.

Fuino, L., Bali, P., Wittmann, S., Donapaty, S., Guo, F., Yamaguchi, H., Wang, H.G., Atadja, P., Bhalla, K., 2003. Histone deacetylase inhibitor LAQ824 down-regulates Her-2 and sensitizes human breast cancer cells to trastuzumab, taxotere, gemcitabine, and epothilone B. Mol. Cancer Therapeut. 2, 971–984.

Gatla, H.R., Muniraj, N., Thevkar, P., Yavvari, S., Sukhavasi, S., Makena, M.R., 2019. Regulation of chemokines and cytokines by histone deacetylases and an update on histone decetylase inhibitors in human diseases. Int. J. Mol. Sci. 20, 1110.

Grabiec, A.M., Potempa, J., 2018. Epigenetic regulation in bacterial infections: targeting histone deacetylases. Crit. Rev. Microbiol. 44, 336–350.

Haggarty, S.J., Koeller, K.M., Wong, J.C., Grozinger, C.M., Schreiber, S.L., 2003. Domain-selective small-molecule inhibitor of histone deacetylase 6 (HDAC6)-mediated tubulin deacetylation. Proc. Natl. Acad. Sci. U. S. A. 100, 4389–4394.

Hubbert, C., Guardiola, A., Shao, R., Kawaguchi, Y., Ito, A., Nixon, A., Yoshida, M., Wang, X.F., Yao, T.P., 2002. HDAC6 is a microtubule-associated deacetylase. Nature 417, 455–458.
Hull, E.E., Montgomery, M.R., Leyva, K.J., 2016. HDAC inhibitors as epigenetic regulators of the immune system: impacts on cancer therapy and inflammatory diseases. BioMed Res. Int. 2016, 8797206.
Kamemura, K., Ogawa, M., Ohkubo, S., Ohtsuka, Y., Shitara, Y., Komiya, T., Maeda, S., Ito, A., Yoshida, M., 2012. Depression of mitochondrial metabolism by downregulation of cytoplasmic deacetylase, HDAC6. FEBS Lett. 586, 1379–1383.
Kato, Y., Salumbides, B.C., Wang, X.F., Qian, D.Z., Williams, S., Wei, Y., Sanni, T.B., Atadja, P., Pili, R., 2007. Antitumor effect of the histone deacetylase inhibitor LAQ824 in combination with 13-cis-retinoic acid in human malignant melanoma. Mol. Cancer Therapeut. 6, 70–81.
Kawaguchi, Y., Kovacs, J.J., McLaurin, A., Vance, J.M., Ito, A., Yao, T.P., 2003. The deacetylase HDAC6 regulates aggresome formation and cell viability in response to misfolded protein stress. Cell 115, 727–738.
Kukavica-Ibrulj, I., Facchini, M., Cigana, C., Levesque, R.C., Bragonzi, A., 2014. Assessing Pseudomonas aeruginosa virulence and the host response using murine models of acute and chronic lung infection. Methods Mol. Biol. 1149, 757–771.
Lam, H.C., Cloonan, S.M., Bhashyam, A.R., Haspel, J.A., Singh, A., Sathirapongsasuti, J.F., Cervo, M., Yao, H., Chung, A.L., Mizumura, K., An, C.H., Shan, B., Franks, J.M., Haley, K.J., Owen, C.A., Tesfaigzi, Y., Washko, G.R., Quackenbush, J., Silverman, E.K., Rahman, I., Kim, H.P., Mahmood, A., Biswal, S.S., Ryter, S.W., Choi, A.M., 2013. Histone deacetylase 6-mediated selective autophagy regulates COPD-associated cilia dysfunction. J. Clin. Invest. 123, 5212–5230.
Lee, J.H., Yao, Y., Mahendran, A., Ngo, L., Venta-Perez, G., Choy, M.L., Breslow, R., Marks, P.A., 2015. Creation of a histone deacetylase 6 inhibitor and its biological effects. Proc. Natl. Acad. Sci. U. S. A. 112, 12005–12010.
Li, Y., Zhao, T., Liu, B., Halaweish, I., Mazitschek, R., Duan, X., Alam, H.B., 2015. Inhibition of histone deacetylase 6 improves long-term survival in a lethal septic model. J. Trauma Acute Care Surg. 78, 378–385.
Licciardi, P.V., Karagiannis, T.C., 2012. Regulation of immune responses by histone deacetylase inhibitors. ISRN Hematol 2012, 690901.
Lu, B., Li, L., Schneider, M., Hodges, C.A., Cotton, C.U., Burgess, J.D., Kelley, T.J., 2019. Electrochemical measurement of membrane cholesterol correlates with CFTR function and is HDAC6-dependent. J. Cyst. Fibros. 18, 175–181.
Moutin, M.J., Bosc, C., Peris, L., Andrieux, A., 2021. Tubulin post-translational modifications control neuronal development and functions. Dev. Neurobiol. 81, 253–272.
Nichols, D.P., Chmiel, J.F., 2015. Inflammation and its genesis in cystic fibrosis. Pediatr. Pulmonol. 50, S39–S56.
Nusinzon, I., Horvath, C.M., 2003. Interferon-stimulated transcription and innate antiviral immunity require deacetylase activity and histone deacetylase 1. Proc. Natl. Acad. Sci. U.S.A. 100, 14742–14747.
Ran, J., Zhou, J., 2019. Targeted inhibition of histone deacetylase 6 in inflammatory diseases. Thorac. Cancer 10, 405–412.
Ren, Y., Su, X., Kong, L., Li, M., Zhao, X., Yu, N., Kang, J., 2016. Therapeutic effects of histone deacetylase inhibitors in a murine asthma model. Inflamm. Res. 65, 995–1008.
Rosenjack, J., Hodges, C.A., Darrah, R.J., Kelley, T.J., 2019. HDAC6 depletion improves cystic fibrosis mouse airway responses to bacterial challenge. Sci. Rep. 9, 10282.
Rymut, S.M., Harker, A., Corey, D.A., Burgess, J.D., Sun, H., Clancy, J.P., Kelley, T.J., 2013. Reduced microtubule acetylation in cystic fibrosis epithelial cells. Am. J. Physiol. Lung Cell Mol. Physiol. 305, L419–L431.
Rymut, S.M., Corey, D.A., Valerio, D.M., Erokwu, B.O., Flask, C.A., Kelley, T.J., Hodges, C.A., 2017. Improved growth patterns in cystic fibrosis mice after loss of histone deacetylase 6. Sci. Rep. 7, 3676.
Shan, B., Yao, T.P., Nguyen, H.T., Zhuo, Y., Levy, D.R., Klingsberg, R.C., Tao, H., Palmer, M.L., Holder, K.N., Lasky, J.A., 2008. Requirement of HDAC6 for transforming growth factor-beta1-induced epithelial-mesenchymal transition. J. Biol. Chem. 283, 21065–21073.
Shen, S., Benoy, V., Bergman, J.A., Kalin, J.H., Frojuello, M., Vistoli, G., Haeck, W., Van Den Bosch, L., Kozikowski, A.P., 2016. Bicyclic-capped histone deacetylase 6 inhibitors with improved activity in a model of axonal Charcot-Marie-tooth disease. ACS Chem. Neurosci. 7, 240–258.
Song, H., Lee, C., Kwak, D., Lee, J., Bae, S., Kim, Y., Bae, D., Ha, N., Bae, M., Kim, J., 2015. Novel Compounds as Histone Deacetylase 6 Inhibitors and Pharmaceutical Compositions Comprising the Same. 137750.
Song, Y., Brady, S.T., 2015. Post-translational modifications of tubulin: pathways to functional diversity of microtubules. Trends Cell Biol. 25, 125–136.
Vij, N., Mazur, S., Zeitlin, P.L., 2009. CFTR is a negative regulator of NFkappaB mediated innate immune response. PLoS One 4, e4664.
Vishwakarma, S., Iyer, L.R., Muley, M., Singh, P.K., Shastry, A., Saxena, A., Kulathingal, J., Vijaykanth, G., Raghul, J., Rajesh, N., Rathinasamy, S., Kachhadia, V., Kilambi, N., Rajgopal, S., Balasubramanian, G., Narayanan, S., 2013. Tubastatin, a selective histone deacetylase 6 inhibitor shows anti-inflammatory and anti-rheumatic effects. Int. Immunopharm. 16, 72–78.
Vlasakova, J., Novakova, Z., Rossmeislova, L., Kahle, M., Hozak, P., Hodny, Z., 2007. Histone deacetylase inhibitors suppress IFN-alpha-induced up-regulation of promyelocytic leukemia protein. Blood 109, 1373–1380.
Wagner, C.J., Schultz, C., Mall, M.A., 2016. Neutrophil elastase and matrix metalloproteinase 12 in cystic fibrosis lung disease. Mol. Cell. Pediatr. 3, 25.
Westermann, S., Weber, K., 2003. Post-translational modifications regulate microtubule function. Nat. Rev. Mol. Cell Biol. 4, 938–947.
Wloga, D., Joachimiak, E., Fabczak, H., 2017. Tubulin post-translational modifications and microtubule dynamics. Int. J. Mol. Sci. 18, 2207.
Worlitzsch, D., Tarran, R., Ulrich, M., Schwab, U., Cekici, A., Meyer, K.C., Birrer, P., Bellon, G., Berger, J., Weiss, T., Botzenhart, K., Yankaskas, J.R., Randell, S., Boucher, R.C., Doring, G., 2002. Effects of reduced mucus oxygen concentration in airway Pseudomonas infections of cystic fibrosis patients. J. Clin. Invest. 109, 317–325.
Yan, B., Liu, Y., Bai, H., Chen, M., Xie, S., Li, D., Liu, M., Zhou, J., 2017. HDAC6 regulates IL-17 expression in T lymphocytes: implications for HDAC6-targeted therapies. Theranostics 7, 1002–1009.
Zhang, X.H., Qin, M., Wu, H.P., Khamis, M.Y., Li, Y.H., Ma, L.Y., Liu, H.M., 2021. A review of progress in histone deacetylase 6 inhibitors research: structural specificity and functional diversity. J. Med. Chem. 64, 1362–1391.
Zhao, T., Li, Y., Liu, B., Pan, B., Cheng, X., Georgoff, P., Alam, H.B., 2016. Inhibition of histone deacetylase 6 restores innate immune cells in the bone marrow in a lethal septic model. J. Trauma Acute Care Surg. 80, 34–40. . discussion 40-1.
Zobell, J.T., Young, D.C., Waters, C.D., Stockmann, C., Ampofo, K., Sherwin, C.M., Spigarelli, M.G., 2012. Optimization of anti-pseudomonal antibiotics for cystic fibrosis pulmonary exacerbations: I. aztreonam and carbapenems. Pediatr. Pulmonol. 47, 1147–1158.